Noninvasive vascular elastography for carotid artery characterization on subjects without previous history of atherosclerosis

Roch L. Maurice
Laboratory of Biorheology and Medical Ultrasonics, Research Center (CRCHUM), University of Montreal Hospital, Montreal, Quebec H2L 2W5, Canada, Institute of Biomedical Engineering, University of Montreal, Montreal, Quebec H3C 3J7, Canada, and Department of Radiology, Radio-Oncology and Nuclear Medicine, University of Montreal, Montreal, Quebec H3C 3J7, Canada

Gilles Soulez
Institute of Biomedical Engineering, University of Montreal, Montreal, Quebec H3C 3J7, Canada, Department of Radiology, University of Montreal Hospital, Montreal, Quebec H2L 4M1, Canada, and Department of Radiology, Radio-Oncology and Nuclear Medicine, University of Montreal, Montreal, Quebec H3C 3J7, Canada

Marie-France Giroux
Department of Radiology, University of Montreal Hospital, Montreal, Quebec H2L 4M1, Canada

Guy Cloutier[a)]
Laboratory of Biorheology and Medical Ultrasonics, Research Center (CRCHUM), University of Montreal Hospital, Montreal, Quebec H2L 2W5, Canada, Institute of Biomedical Engineering, University of Montreal, Montreal, Quebec H3C 3J7, Canada, and Department of Radiology, Radio-Oncology and Nuclear Medicine, University of Montreal, Montreal, Quebec H3C 3J7, Canada

Background: Noninvasive vascular ultrasound elastography (NIVE) was recently introduced to assess mechanical properties (strain or elasticity) of peripheral vessel walls. The goal of this study was to determine strain values in subjects with normal carotid arteries and the reproducibility of these measurements. Methods: Sixteen individuals without previous history of carotid atherosclerosis were recruited in four age categories [40–49], [50–59], [60–69], and [70–79] years old. The left and right common and internal carotids (LCC, LIC, RCC, and RIC, respectively) were independently scanned by two radiologists (RAD-A and RAD-B). The axial strain elastograms were computed with the Lagrangian speckle model estimator. Results: Supported by Bland–Altman analyses, strain values between LCC and RCC were found similar with a Pearson correlation coefficient (r) of 0.83 ($p < 0.0001$). Equivalently, a good correlation was found between RAD-A and RAD-B for common carotids with $r = 0.80$ ($p < 0.0001$). Lower strain values ($p < 0.001$) were measured for male common carotids ($1.62 \pm 0.32\%$) than females ($2.21 \pm 0.76\%$). Regarding the internal carotid strain measurements, the correlation was lower between RAD-A and RAD-B with $r = 0.52$ ($p = 0.01$), but drastically decreased between LIC and RIC ($r = 0.16$, nonsignificant). Male internal carotid strain estimates ($p = 0.03$) were lower ($1.48 \pm 0.44\%$) than in females ($1.84 \pm 0.64\%$). Additionally, male common and internal carotid mean elastic moduli varied from 33–106 kPa, whereas it covered a range of 25–67 kPa for females. Female carotids were more elastic (44 ± 17 kPa) than males (58 ± 17 kPa, $p < 0.001$). Conclusion: Strain measurements in common carotids were found reproducible. However, less consistency was observed for the deeper internal carotids. The NIVE imaging method still remains to be validated with pathological cases, but it might provide a unique approach for stroke prevention and characterization of vascular stiffness. © *2008 American Association of Physicists in Medicine.* [DOI: 10.1118/1.2948320]

I. INTRODUCTION

Carotid artery atherosclerosis is a disease that may lead to plaque rupture or fissure and eventually to a stroke. It is known that the development of this pathology is generally associated with local changes in the vascular tissue mechanical properties. Whereas catheter-based endovascular elastography was introduced to assess strain distribution within coronary arteries,[1–4] noninvasive vascular elastography (NIVE) was proposed to investigate superficial vessels such as the carotid.[5–8] In NIVE, time sequences of radio-frequency (RF) or B-mode data are transcutaneously recorded, while the vessel wall is pressurized by the physiological blood flow pulsation. In this new imaging modality, tissue motion can be assessed using one-dimensional (1D) algorithms to provide maps of axial strain distributions (i.e.,

TABLE I. List of male and female subjects per group of age investigated.

Gender	Age group (years)			
	[40–49]	[50–59]	[60–69]	[70–79]
Male	1	4	2	1
Female	3		4	

TABLE II. List of data sets withdrawn from the statistics, along with the supporting reasons.

Radiologist	Gender	Artery	Age	Reason
RAD-A	Male	LCC	[70–79]	Data not recorded
RAD-B	Male	LCC	[40–49]	Data not recorded
RAD-A	Male	LCC	[60–69]	Motion artifact
RAD-A	Male	RCC-RIC	[40–49]	Motion artifact
RAD-B	Female	LCC-LIC	[40–49]	Motion artifact
RAD-A	Female	LCC-LIC	[40–49]	Small plaque
RAD-B	Female	LCC-LIC	[40–49]	Small plaque
RAD-B	Male	LCC-LIC	[50–59]	Small plaque
RAD-B	Male	LIC-RIC	[60–69]	Small plaque
RAD-B	Male	RCC	[70–79]	Small plaque

strain along the ultrasound beam), whereas two-dimensional (2D) methods were suggested to additionally image lateral strain (i.e., strain perpendicular to the ultrasound beam) and shear distributions. The acoustic radiation force impulse imaging,[9,10] which uses short-duration impulses of relatively high energy to generate tissue kinematics, was proposed to deduce local tissue stiffness from relative amplitudes of axial displacements. Local tissue heating may be a concern of this method when applied to vulnerable plaques. Other noninvasive ultrasound-based methods provided arterial compliance and/or distensibility measurements.[11–13]

The NIVE method presented in this article is based on the Lagrangian speckle model estimator (LSME), described in details elsewhere.[6,14] Briefly, the LSME is a 2D-motion estimator that computes the 2D-deformation matrix (Δ), i.e., axial and lateral strains and shears. In a very recent study, the accuracy of each component of Δ was evaluated.[15] Using biomechanical simulation and vessel-mimicking phantom data, the LSME axial strain and shear motion parameters were demonstrated reliable. The current study consists in an additional validation of NIVE. Namely, its reproducibility between radiologists, and between left and right common and internal carotids, is evaluated. Within such a perspective, longitudinal scans of subjects without any carotid artery disease are investigated. Provided that, for longitudinal scans of vessel walls (close to the middle of the transverse orientation), shear values are expected to be very close to zero, results are then reported only for the axial strain (complex shear parameters have clinical relevance mainly for heterogeneous plaques). Strain and elasticity measurements are also reported as a function of gender and age.

II. MATERIALS AND METHODS

II.A. Experimental protocol

Sixteen individuals without known history of cardiovascular or cerebrovascular diseases, carotid plaques, smoking, or diabetes were recruited. They all signed a written informed consent approved by the ethical committee of the University of Montreal Hospital. One female who incidentally was found to have a severe carotid stenosis (>70% in diameter lumen reduction) was withdrawn, leaving 15 subjects for analysis (eight males, seven females). The population, summarized in Table I, was subdivided into four groups of ages: [40–49], [50–59], [60–69], and [70–79] years old. The left and right common and proximal internal carotid arteries (LCC, LIC, RCC, and RIC, respectively) were

scanned by two radiologists (RAD-A and RAD-B) blinded to each other. The sequence of examinations was also randomly attributed.

Table II summarizes the data sets that were withdrawn from the statistics for the following reasons. First, two scans were mistakenly not recorded by RAD-A and RAD-B, respectively. Second, due to strong motion artifacts during data recording, it was not possible to compute reliable strain values for five data sets. Third, during data analysis, ten scans were excluded because small plaques (<30% in diameter lumen reduction) not identified on the baseline examination were found in data scanned either by RAD-A and/or RAD-B. In summary, 77% of the recorded data were used in the current study.

II.B. Experimental setup

First, conventional B-mode and echo-Doppler examinations were performed with a Philips 5000 system (Philips Medical Systems, Bothell, WA) to detect the presence of carotid atherosclerotic plaques. Thereafter, RF data digitized at 40 MHz were recorded with an Ultrasonix RP550 scanner (Ultrasonix Medical Corporation, Burnaby, BC, Canada) by using a 10-MHz frequency transducer (model L14–5/38). The frame rate varied from 19 to 25 RF images/s, depending on the echo depth. Brachial cuff systolic and diastolic blood pressures (SBP and DBP, respectively) as well as the heart rate were measured at the beginning and at the end of each examination.

II.C. The LSME implementation

The LSME that was used to compute elastograms is described elsewhere.[6] The LSME starts with a rigid registration, using 2D cross-correlation analysis, which allows compensating for potential translation movements. Contrarily to conventional correlation-based estimators that use the gradient of the axial displacement to compute the axial strain elastogram, the LSME was formulated as a nonlinear minimization problem that allows assessing the complete 2D-deformation matrix (Δ). Provided that, in the context of atherosclerotic plaque-free subjects, vessel walls are expected to compress and dilate uniformly, only the axial strain (ε_{yy}) was
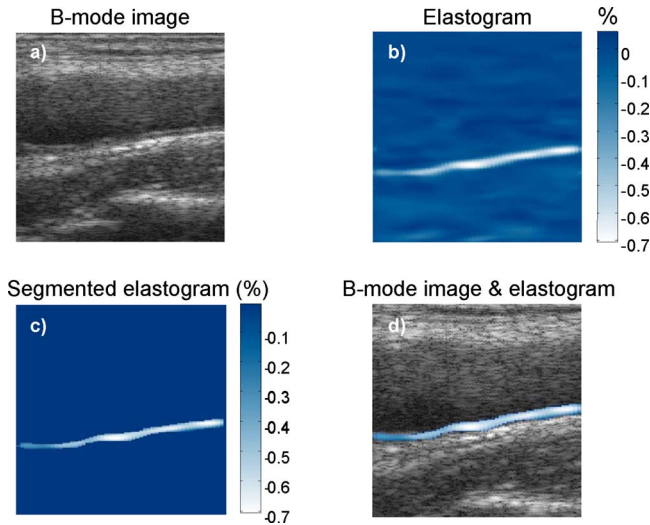
FIG. 1. (a) B-mode image of a left common carotid. (b) Elastogram computed at a given moment of the diastole over the whole image. (c) Manually segmented elastogram of the distal wall. (d) Segmented elastogram superposed on a B-mode image. The elastograms' color-bars give the strain in percent.

FIG. 2. Consecutive instantaneous elastograms computed over a complete cardiac cycle for one male subject's left common carotid. Bright vessel walls (negative strain values) are indicative of vascular tissue dilation and dark walls (positive strains) of vascular compression. From (a) to (p) are mapped elastograms of the diastolic phase, whereas (q) to (w) are for the systolic phase. The elastogram (x) indicates the beginning of a new diastolic phase. Strain values were normalized in a range of −1.5% to +1.5% only for the purpose of qualitative representation.

considered in this study. Additionally, a spatially averaged strain value was calculated from each elastogram of the vessel walls to provide a curve (strain-curve) that is representative of the diastolic/systolic phases of the cardiac cycle (CC). In this context, diastolic strains are negative (dilation of the vessel wall), whereas systolic strains are positive (compression of the wall). Elastograms were computed from each pair of consecutive RF images available within a CC.

The LSME implementation required measurement windows[6] applied on each RF image that were set at 1.53 mm axially by 3.12 mm laterally (80 samples × 20 RF lines), with 90% axial and lateral overlaps. Each RF image measured 25×20 mm² (1296×128 pixels). With the purpose of improving elastograms' signal-to-noise ratio, they were low-pass filtered. The filter was implemented in the frequency domain. Its kernel, which had the same dimension as the elastograms, consisted of a Gaussian whom axial and lateral standard deviations were set to 1 pixel in the frequency domain (which corresponds to 2.80 mm axially by 2.25 mm laterally in the spatial domain).

II.D. Elastogram segmentation

In this study, elastograms were manually segmented to better visualize the vessel wall. Figure 1(a) shows a B-mode image that was acquired from one male subject's LCC. The intima-media layer is clearly delimited at the far wall, but not at the near wall. Figure 1(b) maps the corresponding axial elastogram computed at an arbitrarily selected moment of the diastolic phase over the whole successive RF images of 1296×128 pixels. Similarly to the B-mode image, only the far wall was detected on that elastogram. Owing to that and because clinical protocols on intima-media thicknesses also only consider the far wall,[16] results were restricted to this portion of the carotid artery in this study. Figure 1(c) exhibits

the elastogram in Fig. 1(b) but with the distal wall manually segmented, whereas Fig. 1(d) superposes it on the B-mode image. Because the vessel wall translation motion was generally observed smaller than the wall thickness, the same segmentation mask traced from a diastolic elastogram was applied for the whole RF data set of a given subject. At the exception of three subjects where manual segmentations were tedious for some portions of the wall because of noisy elastograms (due to strong artifactual motions or loss of information at extremities because of lack of ultrasound gel coupling), the whole far wall was segmented and taken into account in the results presented below.

II.E. The strain-curve and the elastic modulus calculation

Figure 2 presents elastograms that were computed over a complete CC for one male subject's LCC. The color-bar gives the strain in percent and was normalized, for the purpose of qualitative comparisons, in a range of −1.5% to +1.5%, with bright vessel walls (negative strain values) indicating vascular tissue dilation and dark vessel walls (positive strains) indicating compression. Figures 2(a)–2(p) are then representative of the diastolic phase, whereas Figs. 2(q)–2(w) represent the systolic phase. The first elastograms of the systole, more specifically Figs. 2(r)–2(t), are a bit noisier due to the instability of the vessel wall at that moment. Nevertheless, at the end-systole [Figs. 2(u)–2(w)], the strain patterns are very coherent indicating a clear compression of the wall. Elastogram of Fig. 2(x) indicates the beginning of a new diastolic phase. It is worth mentioning that vascular tissue compression corresponds to lumen dilation, whereas inversely vascular tissue dilation corresponds to lumen relaxation.

To further introduce the method of calculation of elastic moduli, Fig. 3 exhibits the instantaneous strain-curve that
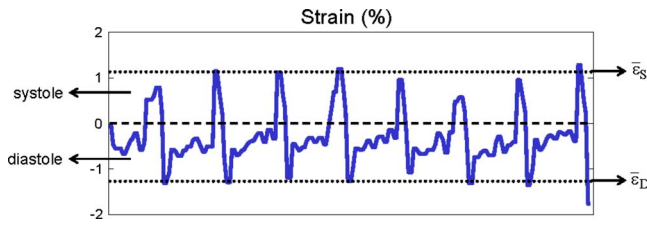
FIG. 3. Strain-curve, for the same male subject's left common carotid reported in Fig. 2, over eight consecutive cardiac cycles. The diastolic and systolic phases are characterized by negative and positive strain values, respectively. $\bar{\varepsilon}_D$ and $\bar{\varepsilon}_S$ define the temporal mean of the peak diastolic and peak systolic values, respectively.

was computed along eight complete CC for the same male subject's LCC presented in Fig. 2. Good reproducibility is observed between CC and furthermore, it can be noted that the temporal mean strain at peak diastole ($\bar{\varepsilon}_D$) and at peak systole ($\bar{\varepsilon}_S$) are about the same in absolute. Provided that artifactual motions are less observed during vascular relaxation,[2] $\bar{\varepsilon}_D$ was selected to calculate the elastic modulus (E_D) that was computed as

$$E_D = \frac{\Delta P}{\bar{\varepsilon}_D}, \quad \text{with:} \quad \Delta P = \frac{\overline{PP}}{\#\text{images}_{\text{diast}} - 1}. \quad (1)$$

In Eq. (1), ΔP defines the pressure gradient between two consecutive RF images. The pulse pressures (PP=SBP−DBP), which were measured with a brachial cuff at the beginning and at the end of each examination, were averaged to provide $\overline{PP}$. Finally, $\#\text{images}_{\text{diast}}$ is the number of RF images within diastole ($\#\text{images}_{\text{diast}} - 1$ elastograms are computed).

III. RESULTS

Figure 3 puts into perspectives both mechanical and physiological interests of NIVE. Regarding physiology, it is worth noting that in the strain-curve, systole lasts, on average, about 1/3 of the whole CC, whereas diastole covers on average about 2/3 of the CC, as it can be expected for a regular heartbeat of 70 pulses/min. In addition, reproducibility of mechanical strain measurements between radiologists and between carotid sides, and comparisons of strains as a function of gender, recording site, and age, were evaluated. To do that, statistics were performed with respect to strains assessed at peak diastole. For convenience and without any lost of generality, the absolute value of the strain was used.

III.A. Comparisons between common and internal carotid artery strain estimations

A first statistical analysis was done to compare the spatially averaged strain $\bar{\varepsilon}_D$ estimates between common and internal carotids, pooling data of RAD-A and RAD-B, left and right sides, and the four groups of ages for males and females. Based on a Mann–Whitney rank sum test, a statistically significant difference was found for strain measurements between both sites ($p=0.014$). Indeed, the common carotid was found to have higher strain estimates (more elas-

tic) with $\bar{\varepsilon}_D = 1.89 \pm 0.63\%$ in comparison to the internal carotid that presented mean strains of $1.63 \pm 0.56\%$. Results for the common and internal carotid arteries are then reported separately.

III.B. Common carotid artery strain estimation

Figure 4(a) shows correlation plot for left and right common carotid (LCC and RCC) strain measurements. The Pearson correlation coefficient (r) was 0.58 ($p<0.01$), but increased to 0.83 ($p<0.0001$) by removing the two points with higher strain values. The corresponding Bland–Altman plot, at Fig. 4(b), exhibits a small bias of $0.04 \pm 1.23\%$ (mean± 2 SD). Similarly, Fig. 4(c) shows the correlation plot for strains measured from common carotids with data recorded by RAD-A and RAD-B, respectively, whereas Fig. 4(d) presents the corresponding Bland–Altman plot with a small bias of $-0.12 \pm 1.06\%$ (mean± 2 SD). The correlation r between radiologists was 0.72 ($p=0.001$), which substantially increased to 0.80 ($p<0.0001$) after removing the two samples with higher strain values. In summary, good concordance was observed for strain values measured (1) between LCC and RCC and (2) between RAD-A and RAD-B for LCC and RCC inclusively.

On the other hand, the Mann–Whitney rank sum test revealed a statistically significant difference between males' and females' common carotid strain estimates ($p<0.001$). Indeed, carotid arteries of males had strains of $1.62 \pm 0.32\%$ versus $2.21 \pm 0.76\%$ for females. Table III summarizes one-way ANOVA tests that were conducted for common carotid arteries. Whereas good concordances were observed between radiologists and recording sides, significant differences between genders and between age groups were found. Such results are argued in discussion.

III.C. Internal carotid artery strain estimation

According to Fig. 5(a), the Pearson correlation coefficient was very low at 0.16 ($p=0.47$), indicating no significant relationships between pair of strain estimates for LIC and RIC. The Bland–Altman plot in Fig. 5(b) exhibits a bias of $0.35 \pm 1.14\%$ (mean± 2 SD). Similarly, Fig. 5(c) shows a fair correlation r of 0.52 ($p=0.01$) between RAD-A and RAD-B, respectively, whereas the Bland–Altman plot in Fig. 5(d) exhibits a bias of $0.23 \pm 1.17\%$ (mean± 2 SD). The Mann–Whitney rank sum test indicated a statistically significant difference between RAD-A and RAD-B for internal carotid scanning ($p=0.03$). In summary, strain values measured between LIC and RIC, and between RAD-A and RAD-B for LIC and RIC inclusively, were not found very similar. The main reasons behind such discrepancies are reported in discussion.

Similarly to common carotids, the Mann–Whitney rank sum test showed a statistically significant difference between males' and females' internal carotid strain estimates. Indeed, male carotids strain values were $1.48 \pm 0.44\%$ compared to females that had mean strains of 1.84 ± 0.64 ($p=0.03$). Table IV summarizes one-way ANOVA results that were obtained for internal carotid arteries. Significant statistical discor-
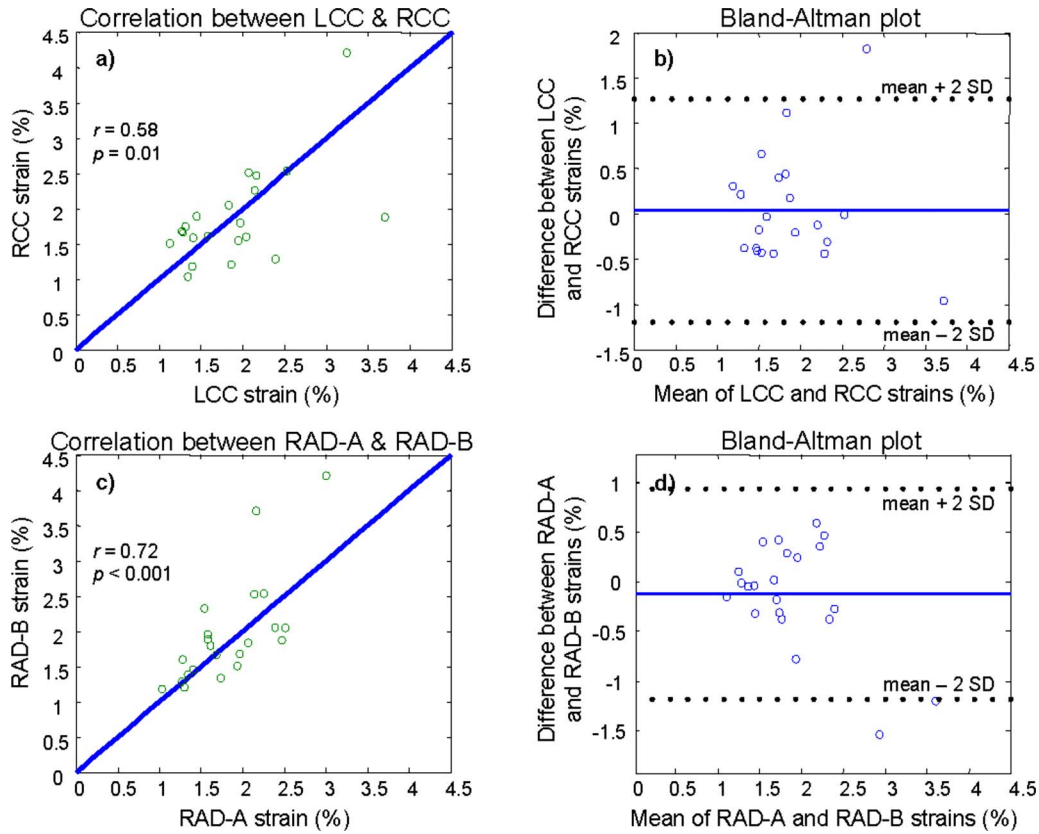
FIG. 4. (a) Correlation plot between LCC and RCC strain measurements; (b) Bland–Altman plot for LCC and RCC strain measurements; (c) Correlation plot between RAD-A and RAD-B, for LCC and RCC strain measurements; and (d) Bland–Altman plot for RAD-A and RAD-B, relatively to LCC and RCC strain measurements. SD is the standard deviation.

dances, for measurements between radiologists, between sides, and between genders, are argued in Sec. IV.

III.D. Effects of age on strain estimates

Two-way ANOVA showed no statistically significant interactions between age and observers ($p=0.449$), between

TABLE III. Summary of strain estimates for the common carotid artery. SD is the standard deviation. The pulse pressure (PP) was in a range of 48 ± 8 mm Hg for males and 47 ± 9 mm Hg for females.

		Mean strain $\pm$ SD (%)	p
Side	Left	1.91 ± 0.64	$=0.802$
	Right	1.88 ± 0.64	
Gender	Male	1.63 ± 0.33	<0.001
	Female	2.21 ± 0.77	
Age group (years)	[40–49]	1.66 ± 0.34	$=0.031$
	[50–59]	1.66 ± 0.31	
	[60–69]	2.14 ± 0.78	
	[70–79]	1.52 ± 0.40	
Observer	RAD-A	1.81 ± 0.51	$=0.758$
	RAD-B	1.87 ± 0.66	

age and sides ($p=0.718$), and between age and sites ($p=0.609$). On the other hand, there were not enough individuals per gender for the different groups of age to provide reliable statistics. This may at least partially explain the statistics showing that older females between 60 and 69 years old exhibited significantly higher strain values ($2.30 \pm 0.75\%$) than younger females between [40 and 49] with mean strains of 1.54 ± 0.32 ($p<0.001$). The male population showed no statistically significant differences between the four groups of ages ($p=0.66$).

III.E. Elastic modulus estimation

Similarly to the study relative to strain estimation, a first statistical analysis was done to compare elastic moduli E_D between common and internal carotids, pooling data of RAD-A and RAD-B, left and right sides, and the four groups of ages for males and females. One-way ANOVA found no statistically significant difference between common and internal sites, with the common carotid artery being on average slightly more elastic with 51 ± 21 kPa than the internal that showed 51 ± 23 kPa ($p=0.091$). Owing to that, common and internal sites were pooled to perform further statistical analyses. One-way ANOVA also found no statistically significant difference between left and right carotid sides with 51 ± 19 kPa and 55 ± 21 kPa, respectively, ($p=0.459$). Similarly, no significant difference was found between
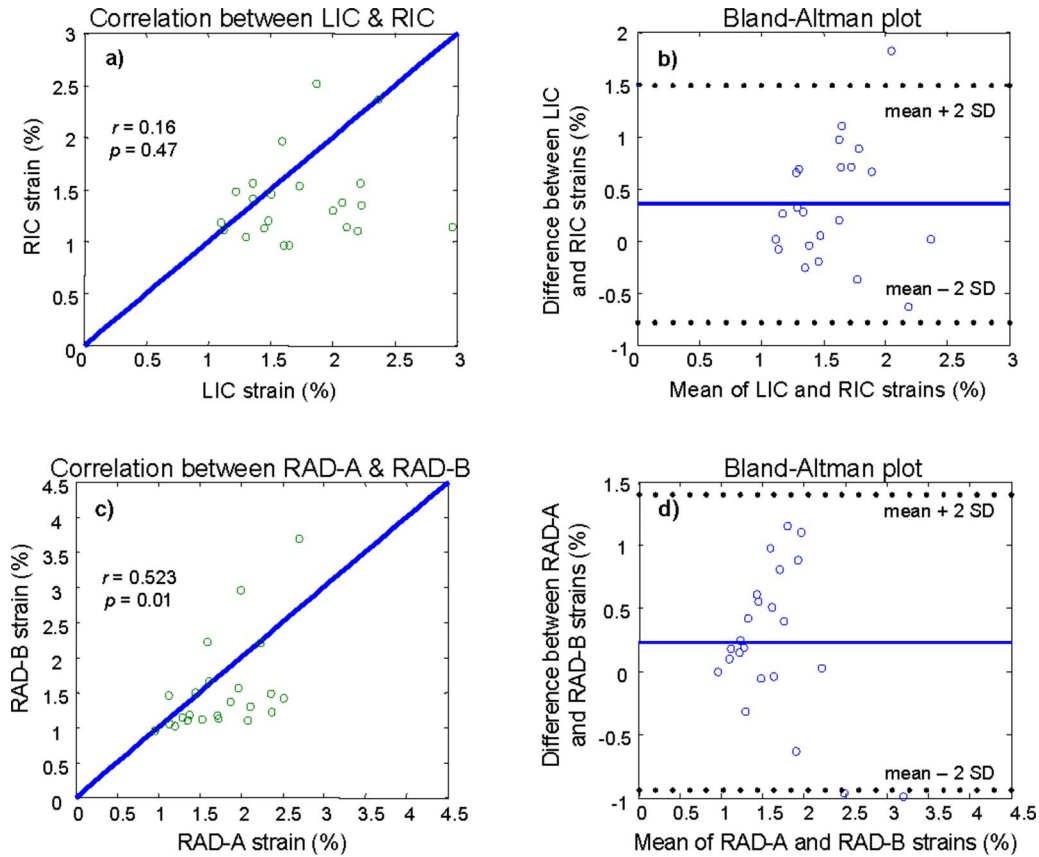
FIG. 5. (a) Correlation plot between LIC and RIC strain measurements; (b) Bland–Altman plot for LIC and RIC strain measurements; (c) Correlation plot between RAD-A and RAD-B, for LIC and RIC strain measurements; and (d) Bland–Altman plot for RAD-A and RAD-B, relatively to LIC and RIC strain measurements.

RAD-A and RAD-B, but elastic moduli estimated from RAD-A's data were found on average lower than those from RAD-B's, with 48 ± 17 kPa and 56 ± 19 kPa, respectively ($p=0.067$). On the other hand, the gender was found to have a statistically significant impact on the elastic moduli, with females' E_D being softer with 44 ± 17 kPa than males' with

58 ± 17 kPa ($p<0.001$) for a population ranging from 40 to 69 years old. Table V summarizes the elastic modulus estimates as a function of gender, side, site, and radiologists.

IV. DISCUSSION

This article reported a human study measuring the strain and elastic modulus of carotid arteries *in vivo* using NIVE. The reproducibility of NIVE was good between radiologists with a correlation coefficient (r) of 0.80 ($p<0.0001$), and also good between left and right sides ($r=0.83, p<0.0001$), with respect to the common carotid artery. On the other hand, consistency regarding the internal carotid was less important. This is mainly explained by the difficulty associated with imaging this deep artery, which is behind the external carotid. Whereas strain estimates may be biased for oblique scans of longitudinal vessels,[17] we noted that it was not always possible to scan internal carotids perpendicular to the ultrasound beam. According to that, motion estimates can be subjected to geometrical distortions that tend to decrease strain estimates (this is similar, by analogy, to angle-dependent Doppler velocity measurements). A solution to this problem would be to apply an angle-dependent strain correction, knowing the angulation of the vessel within the RF image. Finally, motion artifacts may also originate from

TABLE IV. Summary of strain estimates for the internal carotid artery. The PP was in a range of 48 ± 8 mm Hg for males and 47 ± 9 mm Hg for females.

		Mean strain $\pm$ SD (%)	p
Side	Left	1.76 ± 0.46	$=0.038$
	Right	1.56 ± 0.63	
Gender	Male	1.48 ± 0.44	$=0.026$
	Female	1.84 ± 0.65	
Age group (years)	[40–49]	1.45 ± 0.33	$=0.293$
	[50–59]	1.50 ± 0.48	
	[60–69]	1.83 ± 0.68	
	[70–79]	1.72 ± 0.58	
Observer	RAD-A	1.72 ± 0.46	$=0.030$
	RAD-B	1.54 ± 0.66	

TABLE V. Summary of elastic moduli (kPa) for the common and internal carotid arteries.

Gender	Artery	Observer	Age group (years)			
			[40–49]	[50–59]	[60–69]	[70–79]
MALE	LCC	RAD-A	37	59 ± 16	49	-
		RAD-B	-	59 ± 20	58 ± 6	233
	RCC	RAD-A	39	58 ± 9	61 ± 39	
		RAD-B	33	64 ± 16	86 ± 54	408
	LIC	RAD-A	44	49 ± 12	59 ± 23	
		RAD-B	46	75 ± 15	113	120
	RIC	RAD-A	80	64 ± 21	50 ± 18	
		RAD-B	86	79 ± 14	106	280
FEMALE	LCC	RAD-A	61 ± 21		32 ± 9	
		RAD-B	53		36 ± 14	
	RCC	RAD-A	60 ± 23		25 ± 6	
		RAD-B	59 ± 15		47 ± 27	
	LIC	RAD-A	57 ± 10		37 ± 14	
		RAD-B	53		47 ± 13	
	RIC	RAD-A	53 ± 24		33 ± 6	
		RAD-B	65 ± 5		67 ± 47	

patient breathing or swallowing and may be operator-dependent during data acquisition.

IV.A. Regarding the elastic modulus calculation

An elastic modulus calculation strategy was proposed. It takes advantage of the stability of the vessel wall in peak diastole where consecutive RF images are optimally correlated. In addition, with respect to the diastolic phase of the cardiac cycle, peak diastole can be seen as located at the end of the linear portion of the "stress-strain" curve. Owing to that, the linear assumption for the elastic modulus calculation reasonably holds. The gender was found to have an impact on the carotid elasticity, with females' being softer than males'. Interestingly, gender differences were also observed by Riley *et al.*[18] in the atherosclerosis risk in communities study that was conducted over a population of 3321 white male and female individuals between the ages of 45 and 64 years. Nevertheless, their method, being 1D ultrasound based, has concern with lateral resolution and is not supported with qualitative images such as elastograms in the NIVE method. In addition, using B-mode images, methods based on the assessment of the displacement gradient to compute changes in thickness of the carotid wall have been proposed.[19,20] However, to compute the elasticity parameter, such methods require the detection of the luminal boundary of the anterior wall. This may be a very difficult task, because of multiple reflexions from the anterior wall and also scattering from the tissue between the anterior wall and the skin surface.

IV.B. Discussion summary

NIVE was found quite accurate and reproducible with regards to the common carotid. On the other hand, we have reported some pitfalls that could impair NIVE reliability,

namely the potentially angle dependence of our method for internal carotid scanning. In addition, it is to note that the external stress applied by the radiologist with the probe could act as preload on the vessel wall and then impair strain and elasticity estimates.[21] Whereas not of concern in this study because hypertensive subjects were excluded, arterial hypertension also could modulate strain and elastic modulus estimates. Reciprocally, NIVE has the potential for diagnosis and follow-up of patients with hypertension.

Other groups investigated carotid distensibility in atherosclerosis.[22–24] Note that the temporal and spatial mean strain reported in the current study is a measure of distensibility. Namely, Bussy *et al.*[23] investigated common carotid arteries of 40 normal subjects of 47 ± 16 years of age and found an average of 22.6×10^{-3} kPa^{-1} in term of distensibility. Provided distensibility is defined as the inverse of the elastic modulus reported in the current article, this is equivalent to 44 kPa for E_D in Eq. (1). Myers *et al.*[24] reported ranges of 4.2×10^{-3} mm Hg^{-1} (2.9×10^{-3} mm Hg^{-1}) to 2.8×10^{-3} mm Hg^{-1} (2.5×10^{-3} mm Hg^{-1}) for third and fifth decade females' (males') healthy carotid artery, respectively. That is equivalent to 32 kPa (45 kPa) and 47 kPa (53 kPa) in terms of elastic modulus, for the respective populations. Those results are in concordance with the elastic modulus values reported here in Table V, for similar groups of aged subjects. Nonetheless, advantages of the NIVE method stem from its ability to map strain distribution over the whole vessel wall as well as the access to other mechanical properties such as shear (not reported here) whereas distensibility-based methods only provide a single value for the complete wall. For the purpose of investigating atherosclerotic plaques, NIVE can then be seen as a more appropriate method.

V. CONCLUSION

In this article, feasibility and reproducibility of NIVE for the purpose of *in vivo* applications in human carotid arteries were addressed and the ranges of strain values and elastic moduli were given for a normal population. In addition, the reproducibility of NIVE was demonstrated between left and right carotids and between radiologists for the common carotid. On the other hand, results for the internal carotid were less consistent. That is mainly because this vessel is deeply located behind the external carotid and can be scanned only with a certain level of difficulty. We also derived an elastic modulus calculation that, on average, exhibited less than 106 kPa for the vascular disease-free population. Such results are very promising and pave the way to the use of this technique to image and characterize mechanical properties of carotid plaques for stroke prevention.

ACKNOWLEDGMENTS

[a] Author to whom correspondence should be addressed. Present address: Laboratory of Biorheology and Medical Ultrasonics, Research Center (CRCHUM), University of Montreal Hospital, 2099 Alexandre de Sève (room Y-1619), Montréal, Québec H2L 2W5, Canada. Electronic mail: guy.cloutier@umontreal.ca

[1] C. L. de Korte, G. Pasterkamp, A. F. W. Van der Steen, H. A. Woutman, and N. Bom, "Characterization of plaque components with intravascular ultrasound elastography in human femoral and coronary arteries *in vitro*," Circulation **102**, 617–623 (2000).

[2] C. L. de Korte, A. F. W. Van der Steen, E. I. Céspedes, G. Pasterkamp, S. G. Carlier, F. Mastik, A. H. Schoneveld, P. W. Serruys, and N. Bom, "Characterization of plaque components and vulnerability with intravascular ultrasound elastography," Phys. Med. Biol. **45**, 1465–1475 (2000).

[3] É. Brusseau, J. Fromageau, G. Finet, P. Delachartre, and D. Vray, "Axial strain imaging of intravascular data: Results on polyvinyl alcohol cryogel phantoms and carotid artery," Ultrasound Med. Biol. **27**, 1631–1642 (2001).

[4] R. L. Maurice, J. Fromageau, E. Brusseau, G. Finet, G. Rioufol, and G. Cloutier, "On the potential of the Lagrangian speckle model estimator for endovascular elastography: *In vivo* human coronary study," Ultrasound Med. Biol. **33**, 1199–1205 (2007).

[5] J. Bang, T. Dahl, A. Bruinsma, J. H. Kaspersen, T. A. N. Hernes, and H. O. Myhre, "A new method for analysis of motion of carotid plaques from RF ultrasound images," Ultrasound Med. Biol. **29**, 967–976 (2003).

[6] R. L. Maurice, J. Ohayon, Y. Frétigny, M. Bertrand, G. Soulez, and G. Cloutier, "Non-invasive vascular elastography: Theoretical framework," IEEE Trans. Med. Imaging **23**, 164–180 (2004).

[7] H. Ribbers, R. G. Lopata, S. Holewijn, G. Pasterkamp, J. D. Blankensteijn, and C. L. de Korte, "Noninvasive two-dimensional strain imaging of arteries: Validation in phantoms and preliminary experience in carotid arteries *in vivo*," Ultrasound Med. Biol. **33**, 530–540 (2007).

[8] C. Schmitt, G. Soulez, R. L. Maurice, M. F. Giroux, and G. Cloutier, "Non-invasive vascular elastography: Toward a complementary characterization tool of atherosclerosis in carotid arteries," Ultrasound Med. Biol. **33**, 1841–1858 (2007).

[9] G. E. Trahey, M. L. Palmeri, R. C. Bentley, and K. R. Nightingale, "Acoustic radiation force impulse imaging of the mechanical properties of arteries: *In vivo* and *ex vivo* results," Ultrasound Med. Biol. **30**, 1163–1171 (2004).

[10] D. Dumont, R. H. Behler, T. C. Nichols, E. P. Merricks, and C. M. Gallippi, "ARFI imaging for noninvasive material characterization of atherosclerosis," Ultrasound Med. Biol. **32**, 1703–1711 (2006).

[11] M. Safar, *Arteries in Clinical Hypertension* (Lippincott-Raven, Philadelphia, 1996).

[12] E. D. Lehmann, "Terminology for the definition of arterial elastic properties," Pathol. Biol. (Paris) **47**, 656–664 (1999).

[13] M. F. O'Rourke, J. A. Staessen, C. Vlachopoulos, D. Duprez, and G. E. Plante, "Clinical applications of arterial stiffness: Definitions and reference values," Am. J. Hypertens. **15**, 426–444 (2002).

[14] R. L. Maurice and M. Bertrand, "Lagrangian speckle model and tissue-motion estimation—Theory," IEEE Trans. Med. Imaging **18**, 593–603 (1999).

[15] É. Mercure, G. Cloutier, C. Schmitt, and R. L. Maurice, "Performance evaluation of different implementations of the Lagrangian speckle model estimator for non-invasive vascular ultrasound elastography," Med. Phys. (in press).

[16] R. T. Hurst, D. W. C. Ng, C. Kendall, and B. Khandheria, "Clinical use of carotid intima-media thickness: Review of the literature," J. Am. Soc. Echocardiogr. **20**, 907–914 (2007).

[17] É. Mercure, "Non-invasive characterization of blood vessels with ultrasound elastography," M.Sc. dissertation, University of Montreal, 2006.

[18] W. A. Riley, R. W. Barnes, G. W. Evans, and G. L. Burke, "Ultrasonic measurement of the elastic modulus of the common carotid artery: The atherosclerosis risk in communities (ARIC) study," Stroke **23**, 952–956 (1992).

[19] H. Hasegawa, H. Kanai, and Y. Koiwa, "Detection of lumen-intima interface of posterior wall for measurement of elasticity of the human carotid artery," IEEE Trans. Ultrason. Ferroelectr. Freq. Control **51**, 93–108 (2004).

[20] J. K. Balasundaram and R. S. D. W. Banu, "A non-invasive study of alterations of the carotid artery with age using ultrasound images," Med. Biol. Eng. Comput. **44**, 767–772 (2006).

[21] K. Kim, W. F. Weitzel, J. M. Rubin, H. Xie, X. Chen, and M. O'Donnell, "Vascular intramural strain imaging using arterial pressure equalization," Ultrasound Med. Biol. **30**, 761–771 (2004).

[22] C. Giannattasio, M. Failla, G. Emanuelli, A. Grappiolo, L. Boffi, D. Corsi, and G. Mancia, "Local effects of atherosclerotic plaque on arterial distensibility," Hypertension **38**, 1177–1180 (2001).

[23] C. Bussy, P. Boutouyrie, P. Lacolley, P. Challande, and S. Laurent, "Intrinsic stiffness of the carotid arterial wall material in essential hypertensives," Hypertension **35**, 1049–1054 (2000).

[24] C. W. Myers, W. B. Farquhar, D. E. Forman, T. D. Williams, D. L. Dierks, and J. A. Taylor, "Carotid distensibility characterized via the isometric exercise pressor response," Am. J. Physiol. Heart Circ. Physiol. **283**, H2592–H2598 (2002).